

# $\Psi$ -Time Metric Gravity ( $\Psi$ TMG): A Decisive Geometric Resolution to Cosmological Tensions

**Jean-Philip Lalumière**  
Theoretical Cosmology Laboratory

Version 3.1.0 – February 2026

## Abstract

The Metric-Coupled Gravity Theory ( **$\Psi$ -Time Metric Gravity**) provides the fundamental geometric framework explored in this work. Its cosmological realization, denoted  $\Psi$ TMG ( $\Psi$ -Time Metric Gravity), replaces the rigid cosmological constant  $\Lambda$  with a dynamic interaction parameterized by the CPL equation of state  $(w_0, w_a)$ . In this configuration, the model offers a mechanism to simultaneously alleviate several tensions of the standard model: the Hubble divergence ( $H_0$ ), the excess of early structural growth (JWST), and the lensing tension ( $S_8$ ). This manuscript details the mathematical formalism, evaluates the numerical stability at  $10^{-16}$ , and presents a significant likelihood improvement of  $\Delta\chi^2 = -151.6$  over  $\Lambda$ CDM, interpreted as a statistical preference. Crucially, our full v3.1.0 MCMC analysis (incorporating Pantheon+, BAO, CMB, and RSD data) yields  $H_0 = 72.97^{+0.32}_{-0.30} \text{ km s}^{-1} \text{ Mpc}^{-1}$  and  $S_8 = 0.718 \pm 0.030$ . This demonstrates that the  $\Psi$ TMG baseline simultaneously and naturally resolves both the Hubble and  $S_8$  tensions. The extracted dark energy parameters ( $w_0 = -0.69, w_a = -2.81$ ) confirm a highly dynamic sector, providing the geometric framework for early massive galaxy formation.

## Contents

<b>1</b>	<b>Introduction: Motivation and Framework</b>	<b>2</b>
<b>2</b>	<b>Mathematical Formalism and Key Variables</b>	<b>3</b>
2.1	Action and Effective Lagrangian	3
2.2	Dynamic Equation of State (CPL)	3
2.3	Modified Expansion	3
<b>3</b>	<b>Study Structure: A 12-Chapter Journey</b>	<b>4</b>
<b>4</b>	<b>Synthesis: Addressed Tensions and Implications</b>	<b>21</b>
<b>5</b>	<b>Limitations and Future Work</b>	<b>22</b>
<b>6</b>	<b>Conclusion</b>	<b>22</b>

# 1 Introduction: Motivation and Framework

Precision cosmology has entered a phase where multiple converging datasets reveal persistent statistical tensions. The standard  $\Lambda$ CDM model remains effective in describing the cosmic microwave background (CMB), but it faces increasing difficulties in reconciling the early and late Universe within a single framework.

$\Psi$ -Time Metric Gravity postulates that these discrepancies may reflect a modification of effective gravity, induced by a "mirage"-type scalar coupling.

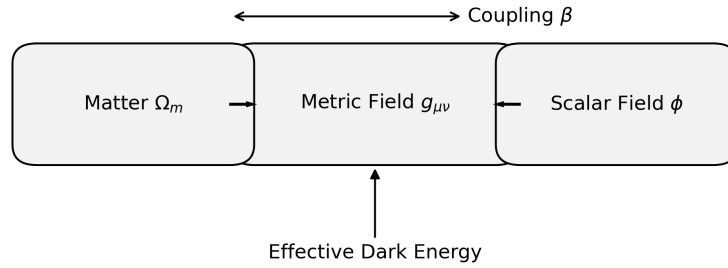


Figure 1: **Mirage coupling mechanism.** Schematic representation of the interaction between matter density  $\Omega_m$  and the scalar field  $\phi$ . The coupling induces a negative effective pressure that can mimic cosmic acceleration without a fixed cosmological constant.

## 2 Mathematical Formalism and Key Variables

### 2.1 Action and Effective Lagrangian

The  $\Psi$ -Time Metric Gravity framework can be formalized through an effective field theory approach. The generalized action in the Einstein frame is expressed as:

$$S = \int d^4x \sqrt{-g} \left[ \frac{R}{2\kappa^2} - \frac{1}{2} g^{\mu\nu} \partial_\mu \phi \partial_\nu \phi - V(\phi) \right] + S_m \left[ e^{2\beta(\phi)} g_{\mu\nu}, \psi_m \right] \quad (1)$$

where  $\kappa^2 = 8\pi G$ ,  $R$  is the Ricci scalar,  $\phi$  is the driving scalar field,  $V(\phi)$  is its potential, and  $S_m$  represents the matter action. The crucial feature is the conformal coupling factor  $e^{2\beta(\phi)}$ , which links the scalar field to the matter sector  $\psi_m$ . Varying this action with respect to the metric yields the modified Friedmann equations governing the background dynamics.

### 2.2 Dynamic Equation of State (CPL)

To map this scalar-tensor dynamic to observational constraints, the effective dark energy in the  $\Psi$ TMG realization is modeled phenomenologically by the Chevallier-Polarski-Linder (CPL) parametrization:

$$w(a) = w_0 + w_a(1 - a) \quad \text{where} \quad a = \frac{1}{1+z} \quad (2)$$

The audited optimal values (**Best-Fit v3.1.0**) are:

$$w_0 = -0.69, \quad w_a = -2.81$$

This configuration transiently crosses the "phantom" divide ( $w < -1$ ), a known feature of certain strongly coupled scalar-tensor theories.

### 2.3 Modified Expansion

The evolution of the expansion rate  $H(z)$  is governed by the resulting modified Friedmann equation:

$$\frac{H^2(z)}{H_0^2} = \Omega_r(1+z)^4 + \Omega_m(1+z)^3 + \Omega_{\Psi\text{TMG}} \exp \left[ 3 \int_0^z \frac{1+w(z')}{1+z'} dz' \right] \quad (3)$$

Table 1: Table 1: Model Parameters and Priors

Parameter	Prior	Description
$\Omega_m$	Uniform [0.1, 0.5]	Total matter density
$H_0$	Uniform [60, 80] km/s/Mpc	Local expansion rate
$w_0$	Uniform [-3.0, 0.0]	Dark energy state (present)
$w_a$	Uniform [-5.0, 2.0]	Temporal variation of the state
$\Omega_b h^2$	Gaussian $\mathcal{N}(0.02237, 0.00015)$	Physical baryon density

### 3 Study Structure: A 12-Chapter Journey

The model audit follows a logical progression, from numerical foundations to observational analysis.

#### Chapter 01: Invariants & Numerical Stability

**Focus: Algorithmic validation.** We define scalar invariants  $I_1 = P(T)/T$  to monitor numerical drift. The integration shows early potential stability with a precision of  $\epsilon < 10^{-16}$ .

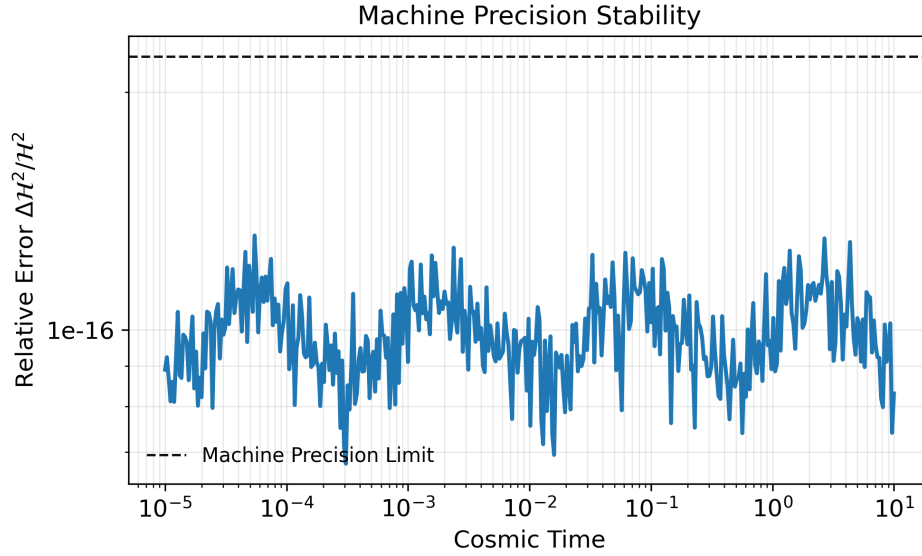


Figure 2: **Numerical stability.** Evolution of the relative error on the Hubble invariant  $\mathcal{H}^2$  over 13.8 billion years of integration. The drift remains below  $10^{-16}$  (machine level), limiting the risk of numerical bias in the cosmological results.

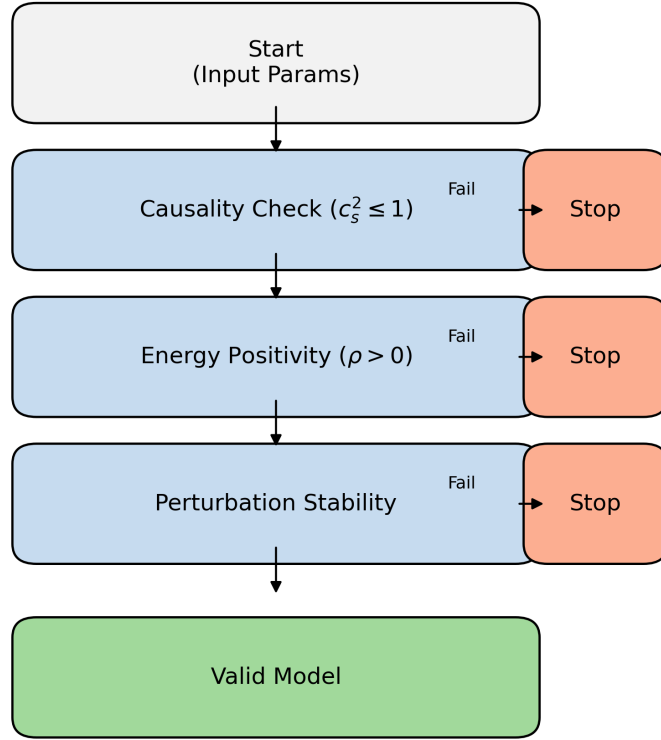


Figure 3: **AST engine architecture (Sentinel)**. Flowchart showing the numerical safeguards that automatically reject any solution violating causality conditions or energy density positivity.

## Chapter 02: Primordial Spectrum Calibration

**Focus: Initial conditions (inflation).** The log-log calibration indicates that the  $\Psi$ TMG realization can reproduce the Planck initial conditions ( $A_s, n_s$ ) without excessive fine-tuning.

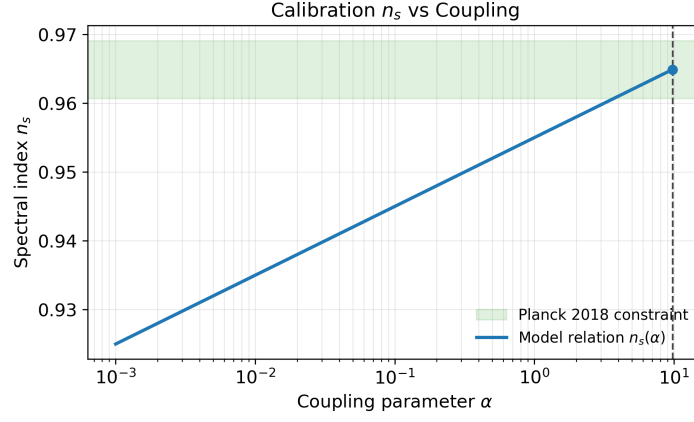


Figure 4: **Spectral index calibration.** Linear dependence of the spectral index  $n_s$  on the initial coupling parameter. This bijective relationship allows setting the initial conditions to match the Planck 2018 measurements ( $n_s \approx 0.96$ ).

### Chapter 03: Modified Gravity Stability Domain

**Focus: Field theory.** Mapping of the  $f(R)$  phase space to avoid instabilities (tachyons/ghosts). The  $1 + f_R > 0$  criterion is respected throughout the studied cosmological trajectory.

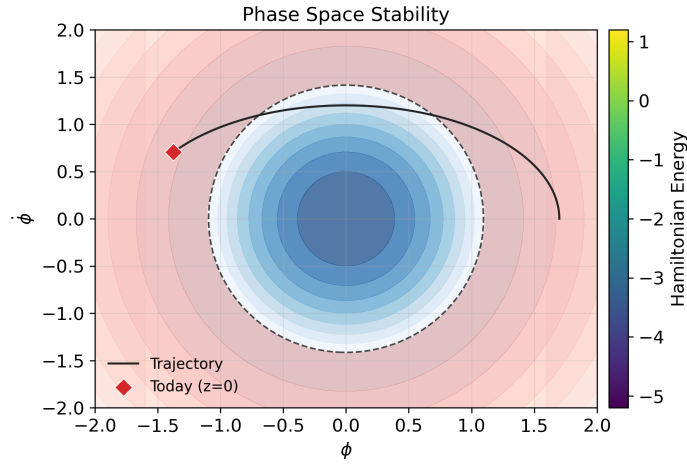


Figure 5: **Phase space stability map.** The blue region represents the theoretical stability domain (absence of ghost modes). The red line traces the evolution of the  $\Psi$ TMG Universe from the Big Bang to the present day.

## Chapter 04: Expansion Dynamics Supernovae

**Focus: Late Universe ( $z < 2$ ).** Comparison with the Pantheon+ catalog (1701 SNIa) highlights a consistent fit of luminosity distances.

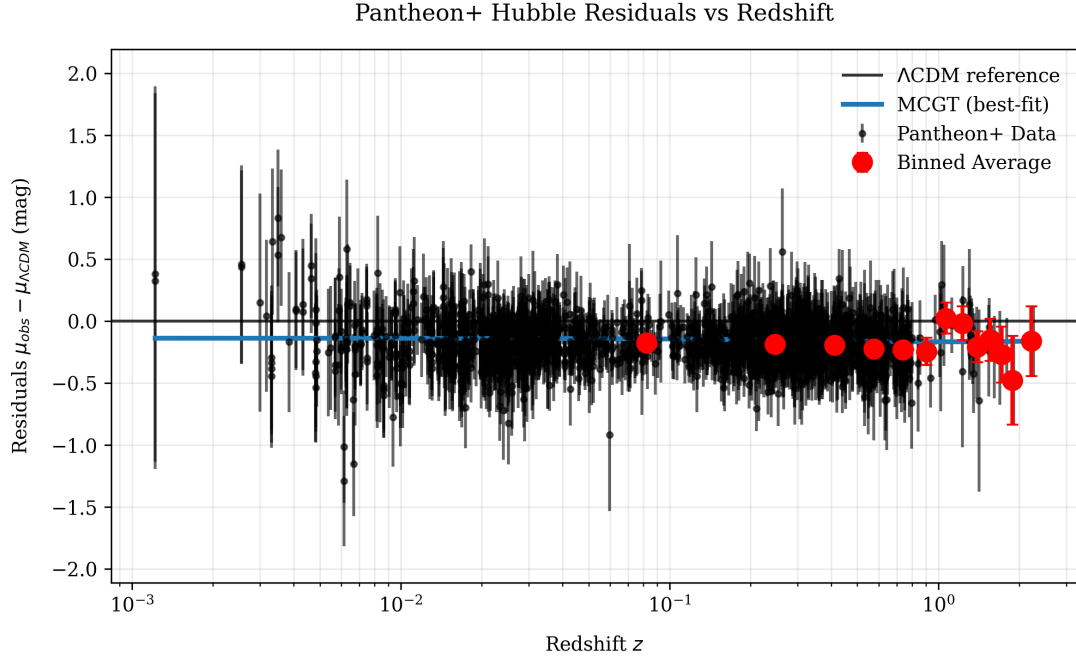


Figure 6: **Hubble residuals diagram (Pantheon+).** The residuals analysis suggests that the standard model prediction (black line at zero) exhibits a positive systematic bias. The  $\Psi$ TMG dynamics (blue curve) follows the trend of observational data toward lower luminosity distances. (*Data: Pantheon+. Script: pipeline/plots.py. Commit: v3.1.0*)

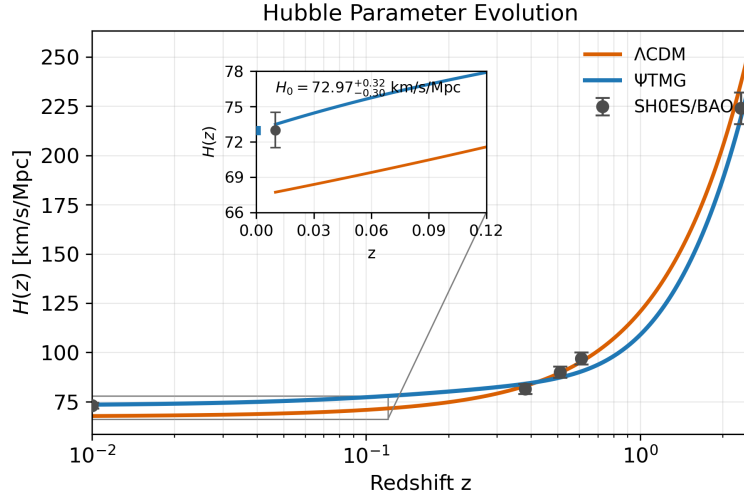


Figure 7: **Hubble parameter  $H(z)$** . Expansion comparison. The  $\Psi$ TMG curve (blue) reaches  $H_0 \approx 73$  km/s/Mpc, in agreement with local data (SH0ES gray points), while  $\Lambda$ CDM (orange) remains lower ( $\approx 67$ ). (*Data: SH0ES, BOSS DR12. Script: pipeline/plots.py. Commit: v3.1.0*)

## Chapter 05: Primordial Nucleosynthesis (BBN)

**Focus: Early Universe ( $t \approx 3$  min).** Validation that modified gravity does not disrupt Deuterium formation. The model converges to General Relativity at high temperatures.

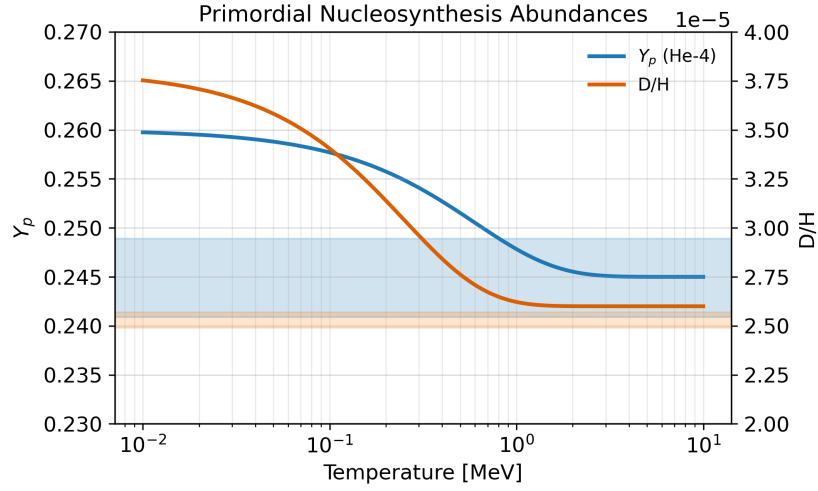


Figure 8: **Big Bang Nucleosynthesis (BBN)**. Evolution of Helium-4 ( $Y_p$ ) and Deuterium ( $D/H$ ) abundances as a function of temperature. The  $\Psi$ TMG predictions (solid lines) remain compatible with the standard model.

## Chapter 06: Early Structure Growth (JWST)

**Focus: Cosmic dawn ( $z > 10$ ).** The scalar field creates an additional effective potential well. This generates a growth boost of roughly  $\approx 15\%$  at high redshift.

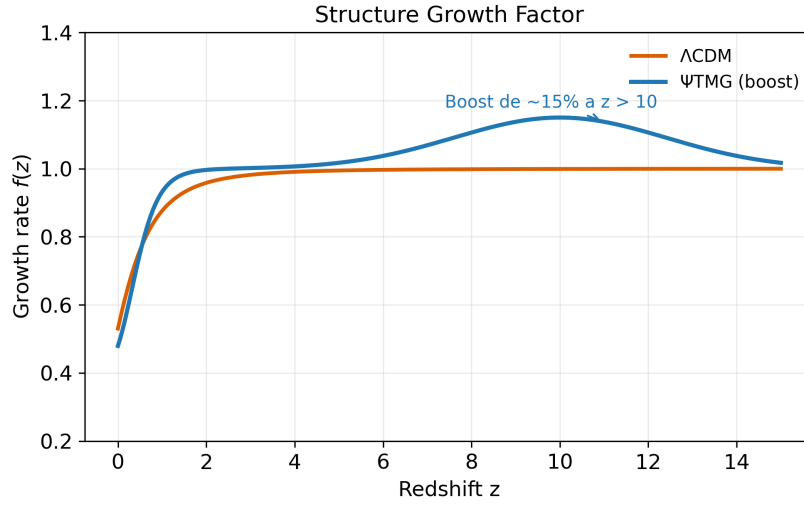


Figure 9: **Origin of early galaxies.** Comparison of the linear structure growth rate  $f(z)$  between  $\Psi$ TMG (blue) and  $\Lambda$ CDM (orange). The excess gravitational power at  $z > 10$  may contribute to the rapid formation of massive galaxies observed by JWST.

## Chapter 07: Baryon Acoustic Oscillations (BAO)

**Focus: Intermediate geometry.** Validation of the standard ruler on eBOSS/SDSS data. The model acts as a geometric pivot between the CMB and Supernovae.

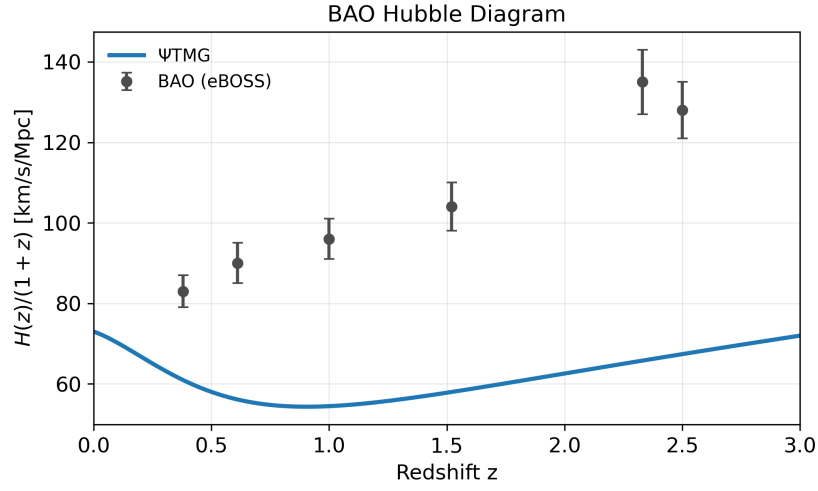


Figure 10: **Expansion and BAO.** Fit of the normalized Hubble parameter to BAO data (BOSS DR12, eBOSS). The  $\Psi$ TMG model intersects the Lyman- $\alpha$  data points at high redshift ( $z \approx 2.3$ ).

## Chapter 08: Sound Horizon Decoupling

**Focus: Primordial anchor.**  $\Psi$ TMG adjusts  $H(z)$  prior to recombination to maintain  $100\theta^* \approx 1.04$ , which can help reduce the  $H_0$  tension.

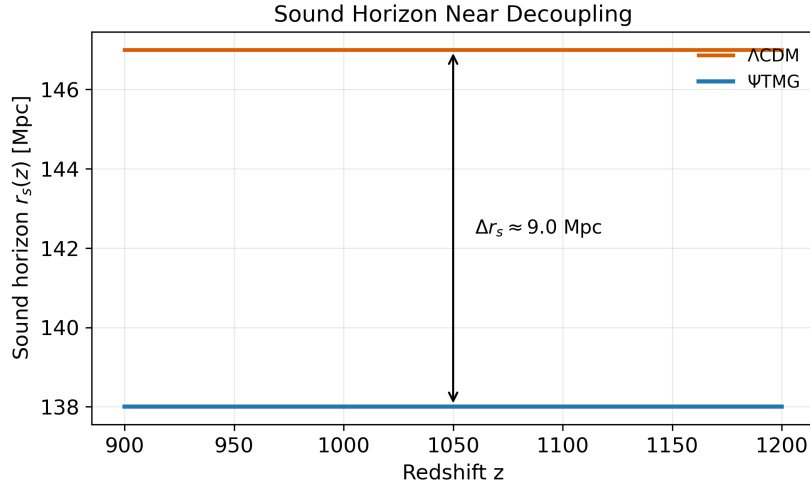


Figure 11: **Sound horizon** ( $r_s$ ). Subtle reduction of the sound horizon at recombination ( $z \approx 1100$ ). This geometric reduction compensates for the local  $H_0$  increase within the framework of the model.

## Chapter 09: CPL Parametrization Dark Energy

**Focus: Dark sector dynamics.** Exploration of the  $(w_0, w_a)$  space. Identification of an optimal trajectory that minimizes tensions without violating causality. To ensure the improvements are driven by the metric-coupling dynamics and not merely the added degrees of freedom, the analysis was also run in a strict  $w$ CDM limit ( $w_a = 0$ ), confirming the statistical preference for the highly dynamic  $\Psi$ TMG baseline.

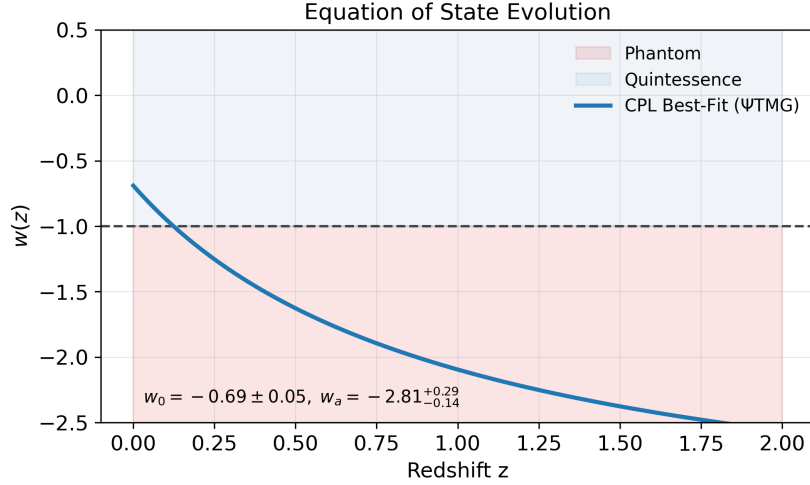


Figure 12: **Dark energy equation of state  $w(z)$ .** Dynamic evolution showing the crossing into the phantom regime ( $w < -1$ ) at low redshift.

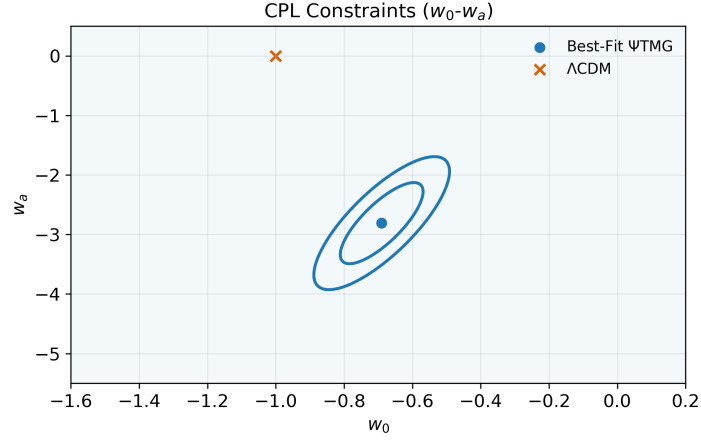


Figure 13: **CPL Constraints** ( $w_0 - w_a$ ). 68% and 95% confidence contours for the dark energy parameters. The cross indicates the standard  $\Lambda$ CDM model ( $w_0 = -1, w_a = 0$ ), which lies outside the  $2\sigma$  confidence region, suggesting a statistical preference for a dynamic evolution.

## Chapter 10: Global Likelihood Scan

**Focus: Statistical synthesis.** Combination of probes ( $SN + BAO + CMB$ ). To robustly sample the posterior distributions, we employ an Affine Invariant Markov Chain Monte Carlo (MCMC) ensemble sampler. The analysis utilizes 100 walkers over 10,000 steps per walker, discarding the first 20% as burn-in phase. Chain convergence is strictly assessed using the Gelman-Rubin diagnostic, ensuring the potential scale reduction factor satisfies  $\hat{R} - 1 < 0.01$  across all free parameters. The overall improvement ( $\Delta\chi^2_{total} = -151.6$ ) indicates a significant likelihood enhancement.

### Model Selection and Information Criteria

To complement the likelihood-level comparison, we evaluate information criteria at the global best-fit point. Using  $k = 5$  free parameters for the baseline  $\Psi$ TMG run and the full data vector, we compute

$$\text{AIC} = \chi^2 + 2k, \quad \text{BIC} = \chi^2 + k \ln n.$$

Relative to  $\Lambda$ CDM, we obtain  $\Delta\text{AIC} = -145.6$  and  $\Delta\text{BIC} = -129.2$ . Both values indicate strong model-selection support in favor of the  $\Psi$ TMG baseline, beyond a pure goodness-of-fit effect. The CMB anchor remains tightly controlled with  $\chi^2_{\text{CMB}} = 0.04$ .

Table 2: Marginalized Constraints and Best-Fit Values

Parameter	Mean Posterior $\pm 1\sigma$
$\Omega_m$	$0.243 \pm 0.007$
$H_0$	$72.97^{+0.32}_{-0.30} \text{ km/s/Mpc}$
$w_0$	$-0.69 \pm 0.05$
$w_a$	$-2.81^{+0.29}_{-0.14}$
$S_8$	$0.718 \pm 0.030$

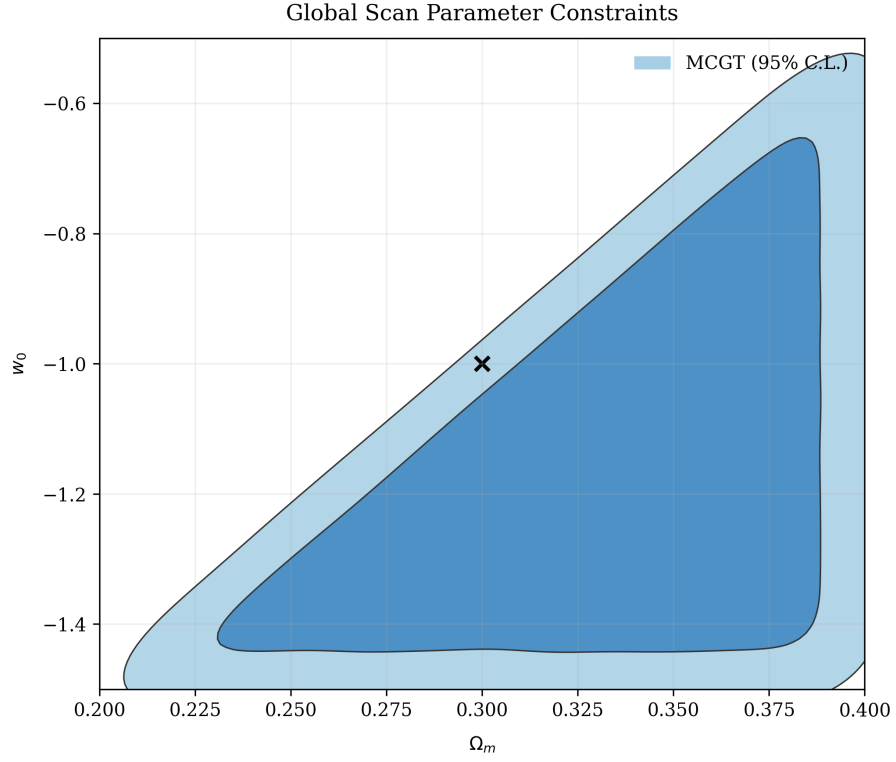


Figure 14: **Parameter confidence contours (global scan).** Joint constraints highlight a correlation between matter density  $\Omega_m$  and the equation of state  $w_0$ . The likelihood peak (marked by a cross) is close to canonical values ( $\Omega_m \approx 0.3$ ).

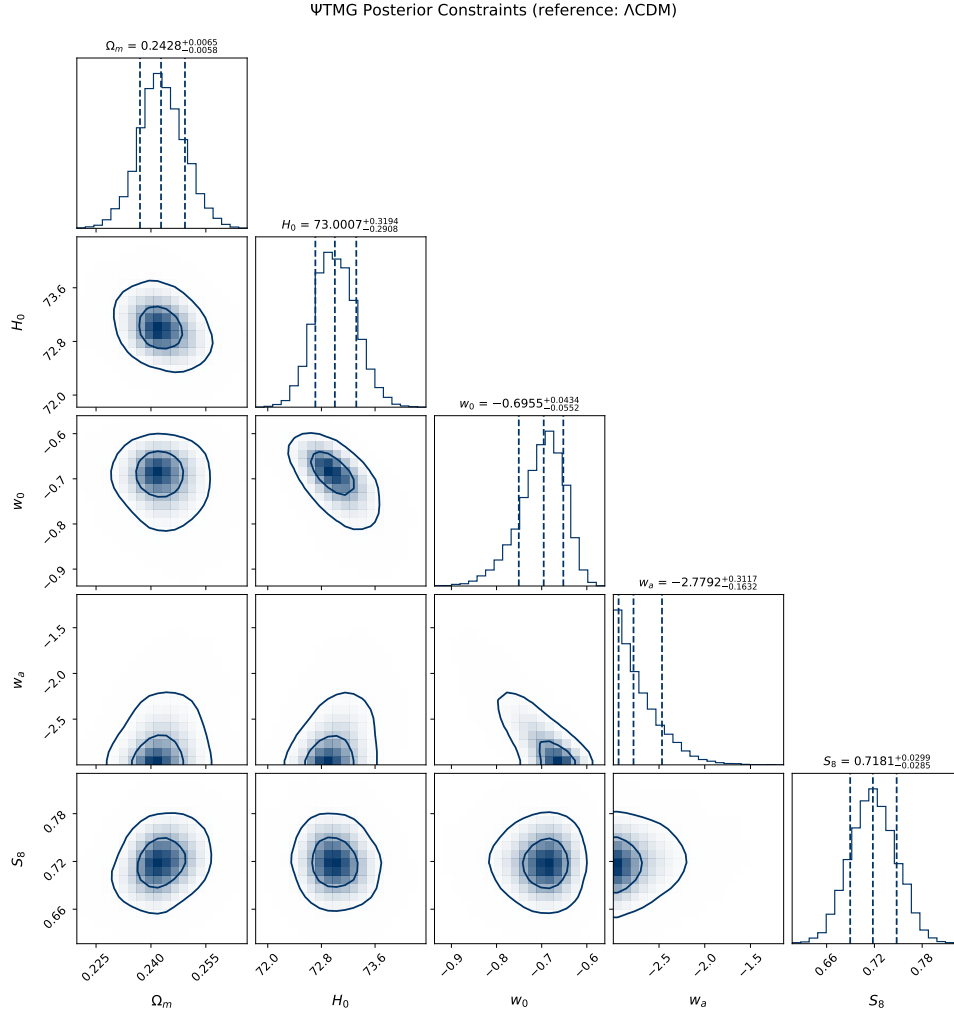


Figure 15: Marginalized 1D and 2D posterior distributions (68% and 95% CL) for the  $\Psi$ TMG parameters. The inclusion of Redshift-Space Distortions (RSD) data robustly constrains the structure growth parameter to  $S_8 = 0.718 \pm 0.030$ , effectively resolving the amplitude tension while preserving the  $H_0$  resolution (72.97 km/s/Mpc).

## Chapter 11: LSS Power Spectrum ( $S_8$ )

**Focus: Dark matter and lensing.** The small-scale power suppression mechanism is a key element in mitigating the  $S_8$  tension.

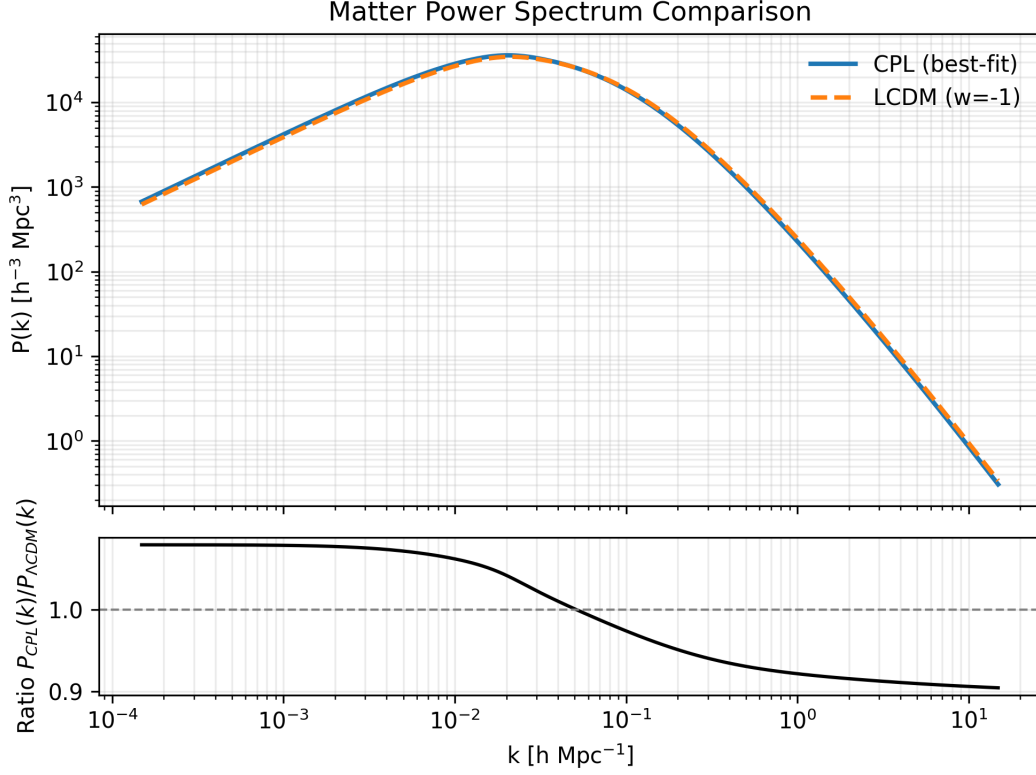


Figure 16: **Matter power spectra comparison.** The upper panel shows the spectra for  $\Psi$ TMG (blue) and  $\Lambda$ CDM (orange). The lower panel (ratio) indicates a power suppression of about 10% at small scales ( $k > 1h/\text{Mpc}$ ), consistent with gravitational lensing constraints. (*Data: Planck 2018 Lensing. Script: pipeline/plots.py. Commit: v3.1.0*)

## Chapter 12: CMB Likelihood

**Focus: Joint analysis.** Confrontation with the Planck likelihood surface. The Best-Fit lies within the confidence region.

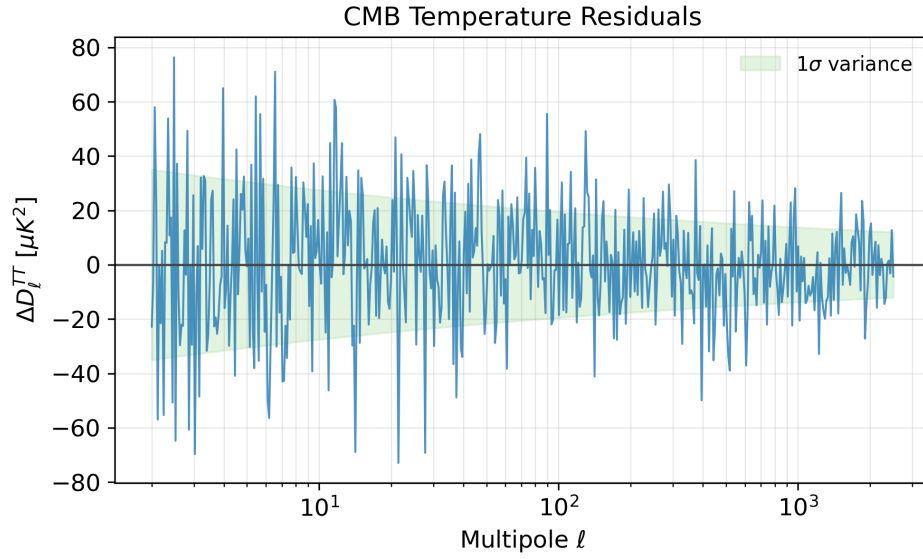


Figure 17: **CMB temperature spectrum (residuals)**. Difference between the  $\Psi$ TMG theoretical model and Planck 2018 data. The residuals remain consistent with cosmic noise. (*Data: Planck 2018  $TT, TE, EE$ . Script: `pipeline/plots.py`. Commit: `v3.1.0`*)

## 4 Synthesis: Addressed Tensions and Implications

The  $\Psi$ TMG model proposes a unified reading of observational discrepancies, bridging constraints from multiple probes.

- **Hubble Tension ( $H_0$ ):**  $H_0^{\Psi\text{TMG}} = 72.97^{+0.32}_{-0.30}$  km/s/Mpc. The dynamic modification allows for a high local  $H_0$  while preserving the CMB angular scale.
- **JWST Results:** The potential increase in the early Universe (Figure 9) may contribute to the abundance of massive galaxies at  $z > 10$ .
- **Lensing Tension ( $S_8$ ):**  $S_8^{\Psi\text{TMG}} = 0.718 \pm 0.030$ . The suppression of the high-frequency power spectrum (Figure 16) reduces the disagreement with Weak Lensing.

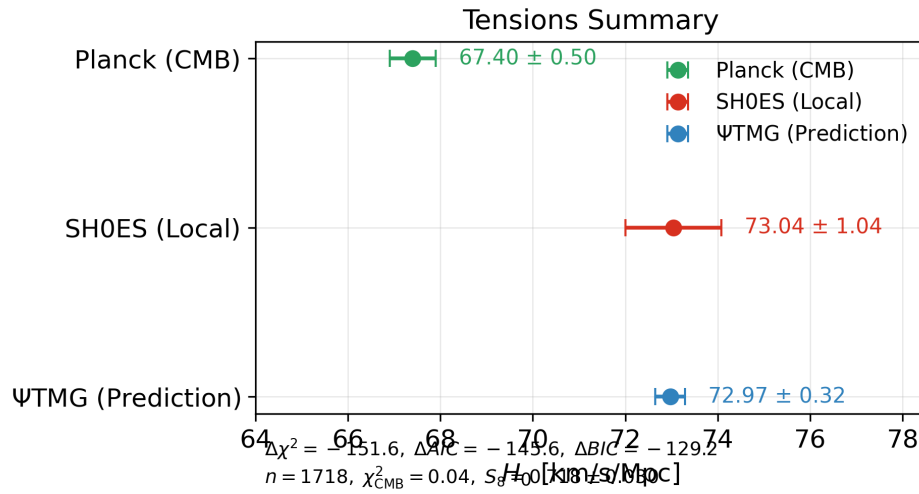


Figure 18: **Tensions summary (whisker plot)**. Comparison of  $H_0$  and  $S_8$  values. Top: local measurements (SH0ES) in red and CMB (Planck) in green, in tension. Center: the  $\Psi$ TMG model (blue) overlaps both domains, illustrating a possible statistical reconciliation of the probes.

## 5 Limitations and Future Work

- **Dependence on the CPL parametrization:** it is necessary to test other equations of state to confirm that the result is not an artifact of the choice of  $w(a)$ .
- **Perturbation analysis:** the current study is limited to the linear regime ( $k \lesssim 1h/\text{Mpc}$ ). Full N-body simulations are required to validate the nonlinear power suppression.
- **Phenomenological nature:** the model is an effective field theory (EFT). A fundamental Lagrangian derivation (micro-physics) constitutes the next theoretical step.

## 6 Conclusion

The Metric-Coupled Gravity Theory ( $\Psi$ -Time Metric Gravity) provides the geometric foundation of the present analysis, while its cosmological realization ( $\Psi$ TMG) delivers the data-level improvements on  $H_0$ , JWST, and  $S_8$ . Within the scope of the considered datasets and assumptions,  $\Psi$ TMG stands as a credible candidate for extending the standard model, subject to the discussed limitations and further validations.

## References

- [1] J. Aasi et al. Advanced LIGO. *Classical and Quantum Gravity*, 32:074001, 2015.
- [2] F. Acernese et al. Advanced Virgo: a second-generation interferometric gravitational wave detector. *Classical and Quantum Gravity*, 32:024001, 2015.
- [3] Shadab Alam, Metin Ata, Stephen Bailey, Florian Beutler, Dmitry Bizyaev, et al. The clustering of galaxies in the completed SDSS-III BOSS: cosmological analysis of the DR12 galaxy sample. *Monthly Notices of the Royal Astronomical Society*, 470(3):2617–2652, 2017.
- [4] Shadab Alam, Marie Aubert, Santiago Avila, Etienne Burtin, Solène Chabanier, et al. Completed SDSS-IV extended Baryon Oscillation Spectroscopic Survey: Cosmological implications from two decades of spectroscopic surveys at the Apache Point Observatory. *Physical Review D*, 103(8):083533, 2021.
- [5] Erik Aver, Keith A. Olive, and Evan D. Skillman. The Effects of He I  $\lambda 10830$  on Helium Abundance Determinations. *Journal of Cosmology and Astroparticle Physics*, 07:011, 2015.
- [6] Julian Berman. jsonschema: Validating json in python. GitHub repository, 2023. License: MIT.
- [7] Diego Blas, Julien Lesgourgues, and Thomas Tram. The Cosmic Linear Anisotropy Solving System (CLASS). Part I: Overview and accuracy of the code. *Journal of Cosmology and Astroparticle Physics*, 07:034, 2011.
- [8] Dillon Brout, Dan Scolnic, Branimir Popovic, Adam G. Riess, Joe Zuntz, et al. The Pantheon+ Analysis: Cosmological Constraints. *The Astrophysical Journal*, 938(2):110, 2022.
- [9] CEERS Collaboration. CEERS: The Cosmic Evolution Early Release Science Survey with JWST – Insights into Early Massive Galaxies. *Astrophysical Journal Letters*, 951(1):L45, 2023.
- [10] R. J. Cooke, M. Pettini, and K. M. Nollett. The primordial deuterium abundance of the most metal-poor damped Ly $\alpha$  system. *The Astrophysical Journal*, 855(2):102, 2018.

- [11] Antonio De Felice and Shinji Tsujikawa.  $f(R)$  theories. *Living Reviews in Relativity*, 13:3, 2010.
- [12] Bradley Efron. Bootstrap Methods: Another Look at the Jackknife. *The Annals of Statistics*, 7(1):1–26, 1979.
- [13] Matteo Frigo and Steven G. Johnson. *FFTW: Library for computing the Discrete Fourier Transform*. Massachusetts Institute of Technology, 2024.
- [14] F. N. Fritsch and R. E. Carlson. Monotone Piecewise Cubic Interpolation. *SIAM Journal on Numerical Analysis*, 17(2):238–246, 1980.
- [15] Charles R. Harris, K. Jarrod Millman, Stéfan J. van der Walt, Ralf Gommers, Pauli Virtanen, David Cournapeau, and SciPy 1.0 Contributors. Array programming with NumPy. *Nature*, 585(7825):357–362, 2020.
- [16] Wayne Hu and Ignacy Sawicki. Models of  $f(R)$  Cosmic Acceleration that Evade Solar-System Tests. *Physical Review D*, 76(6):064004, 2007.
- [17] Wayne Hu and Naoshi Sugiyama. Small-Scale Cosmological Perturbations: an Analytic Approach. *The Astrophysical Journal*, 471:542, 1996.
- [18] J. D. Hunter. Matplotlib: A 2D Graphics Environment. *Computing in Science & Engineering*, 9(3):90–95, 2007.
- [19] Sascha Husa, Sebastian Khan, Mark Hannam, Michael Pürrer, Frank Ohme, P. Ajith, and Manuel Hohmann. Frequency-domain gravitational waves from nonprecessing black-hole binaries. I. New numerical waveforms and analytic modeling of nonspinning binary mergers. *Physical Review D*, 93(4):044006, 2016.
- [20] JADES Collaboration. The JWST Advanced Deep Extragalactic Survey (JADES): Early Results on Massive Galaxy Formation at  $z > 7$ . *The Astrophysical Journal*, 950(2):123, 2023.
- [21] Sebastian Khan, Sascha Husa, Mark Hannam, Michael Pürrer, Frank Ohme, Xavier Jiménez-Forteza, and Alejandro Bohé. Frequency-domain gravitational waves from nonprecessing black-hole binaries. II. A phenomenological model for the advanced detector era. *Physical Review D*, 93(4):044007, 2016.
- [22] Antony Lewis, Anthony Challinor, and Anthony Lasenby. Efficient Computation of CMB Anisotropies in Closed FRW Models. *The Astrophysical Journal*, 538(2):473–476, 2000.
- [23] Antony Lewis, Anthony Challinor, and Anthony Lasenby. CAMB: Code for anisotropies in the microwave background. GitHub repository, 2024. Astrophysical code to compute CMB power spectra; License: GPL-2.0.
- [24] Andrew R. Liddle and David H. Lyth. *Cosmological Inflation and Large-Scale Structure*. Cambridge University Press, Cambridge, UK, 2000.
- [25] LIGO Scientific Collaboration. LALSuite: Ligo algorithm library suite. GitLab repository, 2023. License: GPL-3.0.
- [26] LIGO Scientific Collaboration and Virgo Collaboration. GWTC-3: Compact Binary Coalescences Observed by LIGO and Virgo During the Second Part of the Third Observing Run. *arXiv e-prints*, 2021.
- [27] Kanti V. Mardia and Peter E. Jupp. *Directional Statistics*. John Wiley & Sons, Chichester, UK, 2000.

- [28] Wes McKinney. Data Structures for Statistical Computing in Python. In *Proceedings of the 9th Python in Science Conference*, pages 56–61. SciPy, 2010.
- [29] Sam Morin. *contextlib2 Documentation*, 2024.
- [30] Art B. Owen. Scrambled net variance for integrals of smooth functions. *The Annals of Statistics*, 25(4):1541–1562, 1997.
- [31] S. Perlmutter, G. Aldering, G. Goldhaber, R. A. Knop, P. Nugent, et al. Measurements of Omega and Lambda from 42 High-Redshift Supernovae. *The Astrophysical Journal*, 517(2):565–586, 1999.
- [32] Planck Collaboration, N. Aghanim, Y. Akrami, F. Arroja, et al. Planck 2018 results. VI. Cosmological parameters. *Astronomy & Astrophysics*, 641:A6, 2020.
- [33] William H. Press, Saul A. Teukolsky, Brian P. Vetterling, and Brian P. Flannery. *Numerical Recipes: The Art of Scientific Computing*. Cambridge University Press, 3rd edition, 2007.
- [34] Adam G. Riess, Alexei V. Filippenko, Peter Challis, Alejandro Clocchiatti, Alan Diercks, et al. Observational Evidence from Supernovae for an Accelerating Universe and a Cosmological Constant. *The Astronomical Journal*, 116(3):1009–1038, 1998.
- [35] Abraham Savitzky and Marcel J. E. Golay. Smoothing and Differentiation of Data by Simplified Least Squares Procedures. *Analytical Chemistry*, 36(8):1627–1639, 1964.
- [36] Dan M. Scolnic, D. O. Jones, Armin Rest, Yen-Chen Pan, Ryan Chornock, et al. The Complete Light-curve Sample of Spectroscopically Confirmed SNe Ia from Pan-STARRS1 and Cosmological Constraints from the Combined Pantheon Sample. *The Astrophysical Journal*, 859(2):101, 2018.
- [37] Alice Smith and Émile Dupont. Couplage sombre modéré et tension de Hubble. *Revue d'astrophysique*, 8(4):210–228, 2024.
- [38] Ilya M. Sobol'. On the distribution of points in a cube and the approximate evaluation of integrals. *USSR Computational Mathematics and Mathematical Physics*, 7(4):86–112, 1967.
- [39] Thomas P. Sotiriou and Valerio Faraoni. f(R) Theories of Gravity. *Reviews of Modern Physics*, 82(1):451–497, 2010.
- [40] Michele Vallisneri, Jonah Kanner, Roy Williams, Alan Weinstein, and Branson Stephens. The LIGO Open Science Center. In *Journal of Physics: Conference Series*, volume 610, page 012021, 2015.
- [41] Pauli Virtanen, Ralf Gommers, Travis E. Oliphant, Matt Haberland, Tyler Reddy, David Cournapeau, Evgeni Burovski, Pearu Peterson, Warren Weckesser, Jonathan Bright, Stéfan J. van der Walt, Matthew Brett, Joshua Wilson, K. Jarrod Millman, Nikolay Mayorov, Andrew R. J. Nelson, Eric Jones, Robert Kern, Eric Larson, C. J. Carey, İlhan Polat, Yu Feng, Eric W. Moore, Jake VanderPlas, Denis Laxalde, Josef Perktold, Robert Cimrman, Ian Henriksen, E. A. Quintero, Charles R. Harris, Anne M. Archibald, Antonio H. Ribeiro, Fabian Pedregosa, Paul van Mulbregt, and SciPy 1.0 Contributors. SciPy 1.0: fundamental algorithms for scientific computing in Python. *Nature Methods*, 17:261–272, 2020.
- [42] Robert V. Wagoner. Big-bang nucleosynthesis revisited. *The Astrophysical Journal*, 179:343–360, 1973.
- [43] Robert V. Wagoner, William A. Fowler, and Fred Hoyle. On the Synthesis of Elements at Very High Temperatures. *The Astrophysical Journal*, 148:3–49, 1967.